

Mott transition in Modulated Lattices and Parent Insulator of (K,Tl)Fe_xSe₂ Superconductors

Rong Yu,¹ Jian-Xin Zhu,² and Qimiao Si¹

¹Department of Physics & Astronomy, Rice University, Houston, Texas 77005

²Theoretical Division, Los Alamos National Laboratory, Los Alamos, New Mexico 87545

The degree of electron correlations remains to be a central issue in the iron-based superconductors. The parent iron pnictides and chalcogenides are antiferromagnetic, and their bad-metal behavior has been interpreted in terms of proximity to a Mott transition. We study such a Mott transition in multi-band models on modulated lattices containing an ordered pattern of vacancies, using a slave-rotor method. We show that the ordered vacancies lead to a band-narrowing, which in turn decreases the interaction strength needed for the Mott transition. This effect is proposed to underlie the insulating behavior observed in the parent compounds of the newly discovered (K,Tl)Fe_xSe₂ superconductors.

Introduction. Superconductivity in the layered iron pnictides and chalcogenides occurs at the border of antiferromagnetic order in their parent compounds [1–3]. In their paramagnetic phase, these materials have a large electrical resistivity corresponding to an in-plane carrier mean-free-path on the order of the inverse Fermi wavevector. They also show a strong reduction of the Drude weight [4], and temperature-induced spectral weight transfer that extends to high energies (on the eV order) [5–7]. Such bad-metal behavior is characteristic of metallic systems in proximity to a Mott transition [8–10]

Recently, superconductivity has been discovered in a new family of iron-based compounds KFe_xSe₂ [11] and related (K,Tl)Fe_xSe₂ [12]. While their superconducting transition temperature is as high as in the iron pnictides, these materials are unique in that superconductivity occurs near insulating antiferromagnets in the phase diagram [12]. The control parameter that tunes the system from superconducting to insulating is the Fe composition x , and $x = 1.5$ is the primary candidate composition for a parent compound. There is evidence [12, 13] that (K,Tl)Fe_{1.5}Se₂ has layers of square lattices of irons with ordered vacancies, possibly as illustrated in Figure 1c. Similar properties have also been observed at other Fe concentrations, such as $x = 1.6$ [12]. The in-plane electrical resistivity is about two orders of magnitude larger than that of the iron pnictides at room temperature, and it further increases exponentially as temperature is lowered. The insulating behavior is also manifested in the optical conductivity [14], which is strongly suppressed below about 0.7 eV.

In this letter, we propose that (K,Tl)Fe_{1.5}Se₂ is a Mott insulator arising from a correlation effect that is enhanced by the Fe vacancies. We describe the ordered Fe vacancies in terms of a modulated lattice, and introduce a two-orbital model with two electrons per Fe site to capture their electronic structure. We use a slave-rotor method to show that a Mott transition exists in this model even though there are an even number of electrons per site (and per unit cell). We find that the interaction strength for the Mott transition largely tracks the electronic bandwidth. In other words, ordered Fe vacancies enhance the tendency towards Mott localization as a result of a kinetic-energy reduction. Such Fe vacancies, therefore, have a similar effect as a lattice expansion, which we have previously discussed as responsible for the Mott insulating behav-

ior in La₂O₃Fe₂Se₂ [15]. Our considerations of the interaction effects are realistic, given that the *ab initio* calculations using density-functional theory [16] show that the 3d bands of TlFe_{1.5}Se₂ are narrower than those of TlFe₂Se₂.

Modulated lattices and kinetic-energy reduction. We will consider a square lattice (L1, Fig. 1a), a modulated square lattice describing a square lattice of 2x2 square plaquettes each

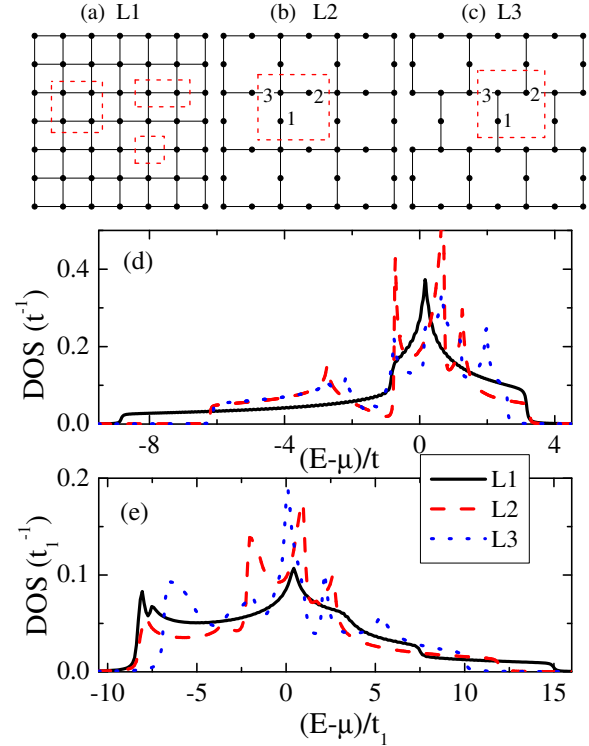


FIG. 1. (Color online) a) Square lattice, L1. Different clusters are used in the slave-rotor calculations, and will be labeled as $N_c = 1, 2$, and 4, respectively; b) Modulated 2x2 square lattice, L2. The enclosed sites 1,2,3 form the basis of the unit cell. Sites 1 and 2 have two neighbors, while site 3 has four; c) Modulated 4x2 square lattice, L3. The enclosed three sites form the basis of the unit cell. Site 1 has two neighbors, and sites 2 and 3 have three. Also shown are the bare density-of-states (DOS) associated with the three lattices for the one-orbital model ($t = t' = 1$) (d) and the two-orbital model (e).

having its center removed (L2, Fig. 1b), and another one corresponding to a triangular lattice of such 2x2 square plaquettes (L3, Fig 1c).

The (K,Tl)Fe_xSe₂ system involves all five 3d orbitals. Both the angle-resolved photoemission experiments [17, 18] and *ab initio* bandstructure calculations using local-density-approximation (LDA) [19–21] show that there are only electron pockets. This is in contrast to the case of iron pnictides, and is easier to model using a two-orbital tight-binding parametrization. Correspondingly, we consider a two-orbital model with the degenerate xz and yz orbitals (labeled as orbitals 1 and 2) and $n = 2$. Inspired by the considerations in the pnictides case [22, 23], we introduce a set of tight-binding parameters. The parameters are listed in Table I, and their meanings can be inferred from the dispersion functions specified in Eq. 2. We first fit the LDA bandstructure obtained on TlFe₂Se₂ to this two-orbital model and then adjust the tight-binding model parameters to give rise to $n = 2$. We notice that the Fermi surface size is larger than in the bandstructure calculations, but this suffices for our qualitative considerations of the effect of lattice depletion on the Mott transition. What is important is that, for the parameters, the Fermi surface comprises only electron pockets near the X points of the 1-Fe per cell Brillouin Zone. The bandwidth narrowing for L2 and L3 lattices compared to the L1 lattice is shown in Fig. 1e.

intra-orbital (eV)				inter-orbital (eV)	
t_1	t_2	t_3	t_9	t_4	t_{12}
0.093	0.081	-0.222	-0.038	0.023	-0.038

TABLE I. Hopping parameters of the two-orbital tight-binding model.

Two-orbital model and the slave-rotor method. We are now in position to specify our model,

$$\mathcal{H} = - \sum_{ij, \alpha, \beta, \sigma} t_{ij}^{\alpha\beta} c_{i\alpha\sigma}^\dagger c_{j\beta\sigma} + \frac{U}{2} \sum_i \left(\sum_{\alpha\sigma} n_{\alpha\sigma} \right)^2 \quad (1)$$

where $c_{i, \alpha, \sigma}$ annihilates an electron in orbital α and spin σ on site i of the Fe lattice. The first term in Eqn. 1 describes the electron hopping, with orbital dependent hopping amplitudes $t_{ij}^{\alpha\beta} = t_1, t_2, \dots, t_{12}$ in the two-orbital model. In the momentum space, this term reads $\sum_{k\alpha\beta\sigma} \epsilon_{k\sigma}^{\alpha\beta} c_{k\alpha\sigma}^\dagger c_{k\beta\sigma}$, where

$$\begin{aligned} \epsilon_k^{11} &= -2t_1 \cos k_x - 2t_2 \cos k_y - 4t_3 \cos k_x \cos k_y \\ &\quad - 4t_9 \cos 2k_x \cos 2k_y, \\ \epsilon_k^{22} &= -2t_2 \cos k_x - 2t_1 \cos k_y - 4t_3 \cos k_x \cos k_y \\ &\quad - 4t_9 \cos 2k_x \cos 2k_y, \\ \epsilon_k^{12} &= \epsilon_k^{21} = -4t_4 \sin k_x \sin k_y - 4t_{12} \sin 2k_x \sin 2k_y. \end{aligned} \quad (2)$$

In this tight-binding Hamiltonian, small hopping between the 5th-nearest neighbors with amplitudes t_9 and t_{12} are included to reproduce the two electron pockets at $n = 2$. The second term in Eqn. 1 is an on-site Coulomb repulsion. We focus

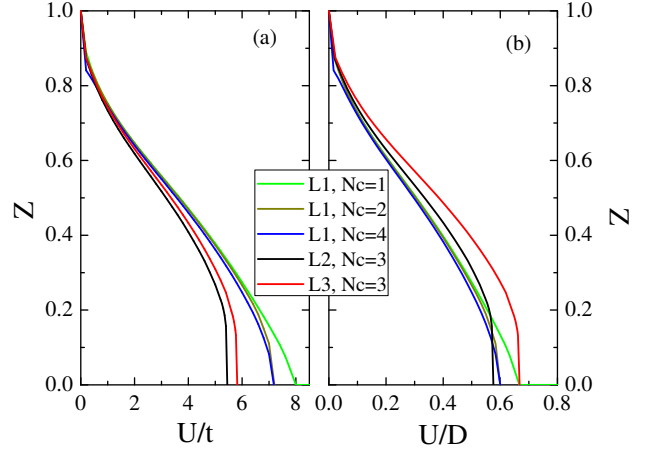


FIG. 2. (Color online) Quasiparticle weight for the one-band model in the unmodulated and modulated lattices plotted as a function of U/t (a) and U/D (b).

on the effect of lattice depletion on the Mott transition and will not consider Hund's coupling and pair-hopping terms for simplicity. All local interactions are expected to have effects similar to U . In particular, the Hund's coupling will reduce the critical U of the Mott transition; its effects are readily studied within a slave-spin method [24, 25], and the results will be reported elsewhere.

We study the model using the cluster slave-rotor mean-field (CSRMF) method [26, 27]. We introduce an $O(2)$ rotor variable θ_i and a spinon $f_{i\alpha\sigma}$ on each site, and rewrite the electron annihilation operator as $c_{i\alpha\sigma} = f_{i\alpha\sigma} e^{-i\theta_i}$. Here, $e^{-i\theta_i}$ lowers the rotor angular momentum L_i , which corresponds to the charge quantum number. The unphysical states are eliminated by enforcing the constraint $L_i = \sum_{\alpha\sigma} (f_{i\alpha\sigma}^\dagger f_{i\alpha\sigma} - 1/2)$ in the enlarged rotor and spinon Hilbert space. By rewriting Eqn.1 using rotor and spinon operators and decoupling the rotor and spinon operators at the mean-field level, we obtain the following two effective Hamiltonians:

$$H_f = - \sum_{ij\alpha\beta\sigma} t_{ij}^{\alpha\beta} C_{ij} f_{i\alpha\sigma}^\dagger f_{j\beta\sigma} - (\mu + \lambda) \sum_{i\alpha\sigma} n_{i\alpha\sigma}^f, \quad (3)$$

$$H_\theta = -2 \sum_{ij} t_{ij}^{\alpha\beta} \chi_{ij}^{\alpha\beta} e^{i(\theta_i - \theta_j)} + \frac{U}{2} \sum_i L_i^2 + \lambda \sum_i L_i, \quad (4)$$

where $C_{ij} \equiv \langle e^{i(\theta_i - \theta_j)} \rangle_\theta$ is the rotor correlation function that renormalizes the quasiparticle hopping parameters in the presence of interaction, $\chi_{ij}^{\alpha\beta} \equiv \langle f_{i\alpha\sigma}^\dagger f_{j\beta\sigma} \rangle_f$, μ is the chemical potential to fix the electron filling in the model, and λ is a Lagrange multiplier to impose the constraint of L_i at the mean-field level. To solve these two Hamiltonians, which still contain interactions among rotors, we further apply a cluster mean-field approximation. We exactly diagonalize the rotor Hamiltonian on a finite cluster, and treat the influence of the sites outside the cluster as a mean field. We decouple $e^{i(\theta_i - \theta_j)}$ into $e^{i\theta_i} \phi_j$ if i belongs to the cluster but j is outside. Here

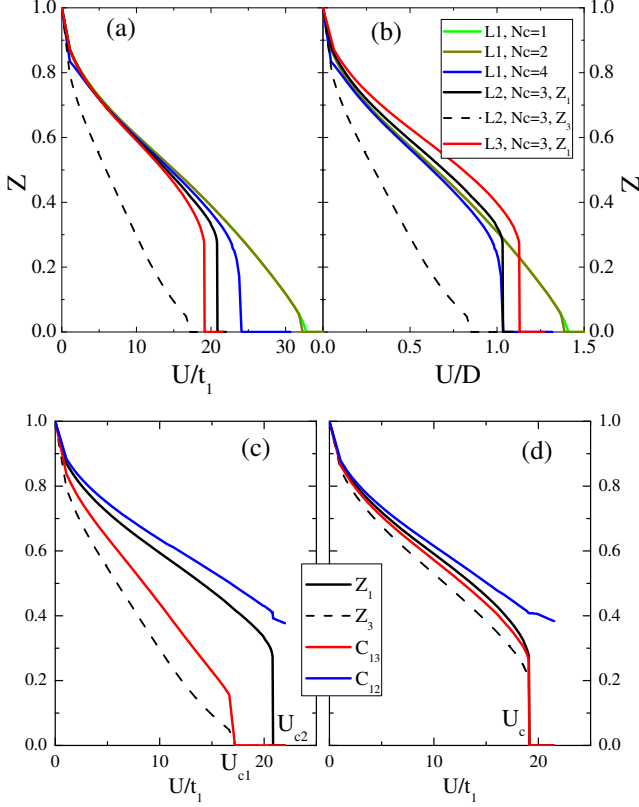


FIG. 3. (Color online) Quasiparticle weight for the two-band model in the unmodulated and modulated lattices plotted as a function of U/t (a) and U/D (b). Also shown are the site-selective quasiparticle weight, Z_1 and Z_3 and the bond correlations for lattices L2 (c) and L3 (d).

$\phi_i \equiv \langle e^{-i\theta_i} \rangle$ is the local mean-field parameter. Consequently, C_{ij} is factorized as $C_{ij} \approx \phi_i^* \phi_j$ if either i or j is outside the cluster. In practice, Eqn. 2 and Eqn. 4 are self-consistently solved by iteratively determining the mean-field parameters ϕ_i , C_{ij} , and $\chi_{ij}^{\alpha\beta}$. The Mott transition is signaled by a vanishing quasiparticle spectral weight $Z = |\phi_i|^2$.

To gain intuition on the role of the lattice modulation, we will also study a one-orbital model with nearest-neighbor hopping, t , and next-nearest-neighbor hopping, t' . Fig. 1d illustrates the reduction of the bandwidth for L2 and L3 lattices from that of the L1 lattice, for the case of $t' = t$. A non-zero t' is chosen for two reasons. It avoids a perfect nesting in the case of $n = 1$, which we study below. It also avoids a flat band in the case of the L2 lattice: when $t' = 0$, for the L2 lattice, there are two dispersive bands with a combined bandwidth of $4\sqrt{2}t$, and a flat band in the middle. A similar band-narrowing effect is illustrated in Fig. 1e for the more realistic two-band model.

Results for the one-orbital model. We start from the one-band case. Because the L2 and L3 lattices involve a 2×2 square plaquette as the unit cell, we will carry out our calculations for the lattice L1 with $N_c = 4$. The slave-rotor mean-

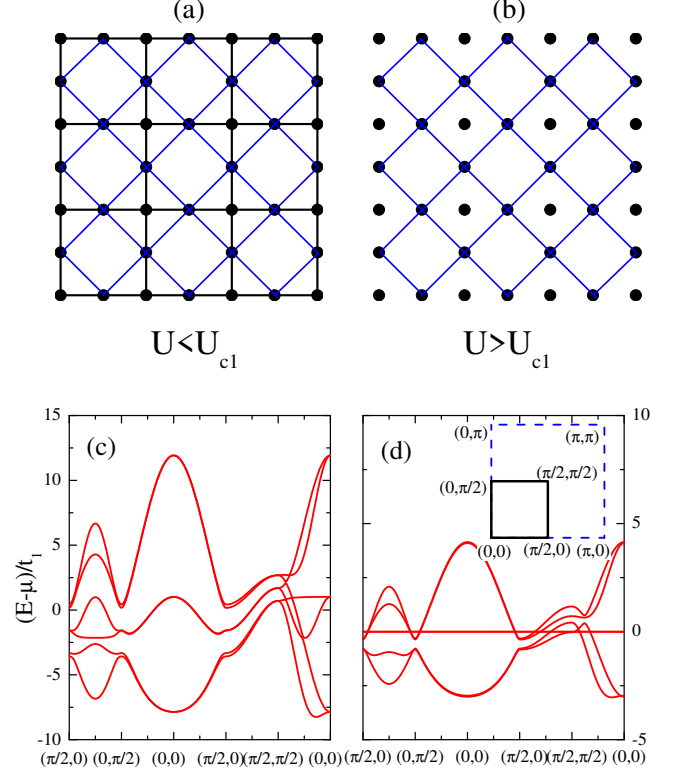


FIG. 4. (Color online) Sketch of the renormalized hoppings for the L2 lattice at $U < U_{c1}$ (a) and at $U_{c1} < U < U_{c2}$ (b). Also shown are the bands of L2 for $U = 0 < U_{c1}$ (c) and for $U_{c1} < U = 19t_1 < U_{c2}$ (d). The bands are shown along the high-symmetry directions in the Brillouin zone associated with the 2×2 Fe unit cell. This Brillouin zone and the zone corresponding to the one Fe cell are illustrated in the inset in (d).

field theory treats the rotor kinetic energy for intra-cluster bonds exactly by diagonalizing the rotor Hamiltonian on the cluster, but treats those of the inter-cluster bonds only within a mean-field approximation. Fig. 2a shows the renormalized quasiparticle weight, Z , as a function of U/t . The Mott transition occurs at U_c , where Z first goes to zero as U is increased. For the L1 lattice, increasing the cluster size from $N_c = 1$ to $N_c = 4$ leads to a successive reduction of U_c : $U_c \approx 8t$ for $N_c = 1$, and $U_c \approx 7.2t$ for $N_c = 4$.

On the modulated lattices, we also find a Mott transition. It is seen that $U_c \approx 5.4t$ for the L2 lattice and $U_c \approx 5.8t$ for L3 lattice, both are smaller than that of the L1 lattice with $N_c = 4$.

Fig. 2b plots the same result, but with U now normalized against the full bandwidth D . It is seen that U_c/D is comparable for all three cases. This clearly illustrates that the reduction of U_c for the modulated L2 and L3 lattices arises from the band-narrowing effect.

Results for the two-orbital model. We now turn to the more realistic two-orbital case. The renormalized quasipar-

ticle weight as a function of U/t_1 is shown in Fig. 3a. It is again seen that the values of U_c for both the L2 and L3 lattices are smaller than that of the L1 lattice with $N_c = 4$.

One difference from the toy 1-band model is that the hopping parameters in the two-orbital model are highly anisotropic. For instance, $t_3/t_2 \approx 3$. The anisotropic hopping makes the local environment possibly different from site to site on the modulated lattices. To fully address the influence of the inhomogeneity, we study the quasiparticle weight associated with each site in the cluster $Z_i = |e^{i\theta_i}|^2$. For either L1 or L3, we obtain a single Mott transition as in the 1-band case. For the L2 lattice, we find two transitions. They are identified by the vanishing of Z_3 first at $U_{c1}/t_1 \approx 17$, and subsequently the vanishing of Z_1 (and equivalently Z_2) at a higher value $U_{c2}/t_1 \approx 20$.

To understand this, we have in the same figure plotted the bond correlators C_{12} and C_{13} . Between U_{c1} and U_{c2} , C_{13} vanishes but C_{12} remains finite. This makes site 3 to be unconnected to the rest of the lattice (*cf.* Fig. 4b). We see these explicitly in a plot of the renormalized bandstructure in Fig. 4d: the isolated 3 sites form a flat band lying exactly on the Fermi level for $U_{c1} < U < U_{c2}$. By contrast, for $U < U_{c1}$, all sites are connected by hopping terms (Fig. 4a) and there exists no flat band (Fig. 4c).

For the L3 lattice, the geometry prevents developing any flat band unless all the hopping parameters are zero. As a result, there will be only one transition. This is clearly seen in comparing Z_1 and Z_3 in Fig. 3d.

The quasiparticle weight as a function of U/D is shown in Fig. 3b. It is again seen that U_c/D is comparable for all three cases. As in the one-band case, this illustrates that the reduction of U_c for the modulated lattices originates from the band-narrowing effect.

Implications for (K,Tl)Fe_xSe₂. Our results imply that the critical interaction strength for the Mott transition will be smaller in (K,Tl)Fe_xSe₂ than in iron arsenides and 11 iron chalcogenides, thereby providing the basis for a Mott-insulating state in the parent (K,Tl)Fe_xSe₂.

The Mott-insulating nature of (K,Tl)Fe_xSe₂ is supported by experiments. As mentioned in the introduction, the materials for both $x = 1.5$ and $x = 1.64$ have large electrical resistivity with an insulating temperature dependence. Furthermore, the insulating behavior in the electrical resistivity is already observed in the paramagnetic phase. Relatedly, the optical conductivity is not only strongly suppressed below about 0.7 eV, but also small in magnitude. For reference, the value of the optical conductivity is compatible to that of the insulating YBa₂Cu₃O_{6+x} with a slight off-stoichiometry $x = 0.2$ [28].

Finally, magnetic order is known to exist in TlFe_xSe₂ at x close to 1.5 [29]. Taken together, these experiments suggest that the insulating state is of the Mott type.

To summarize, we have used a two-orbital model in 1/4-depleted lattices to show that ordered vacancies enhance the tendency for Mott transition, and that this enhancement originates from a vacancy-induced kinetic-energy reduction. Our qualitative conclusion is expected to apply to the more realistic five-orbital model. Based on our calculations, we propose that the insulating parent of the (K,Tl)Fe_xSe₂ superconductors is a Mott insulator at ambient pressure.

We thank J. Dai, M. Fang, and T. Xiang for useful discussions. This work was supported by NSF Grant No. DMR-1006985 and the Robert A. Welch Foundation Grant No. C-1411 (R.Y. and Q.S.), and U.S. DOE at LANL under Contract No. DE-AC52-06NA25396 (J.-X.Z.).

-
- [1] Y. Kamihara *et al.*, J. Am. Chem. Soc., **130**, 3296 (2008).
 - [2] Z. A. Ren *et al.*, Chin. Phys. Lett., **25**, 2215 (2008).
 - [3] C. de la Cruz *et al.*, Nature **453**, 899 (2008).
 - [4] M. M. Qazilbash *et al.*, Nat. Phys. **5**, 647 (2009).
 - [5] W. Z. Hu *et al.*, Phys. Rev. Lett. **101**, 257005 (2008).
 - [6] A. V. Boris *et al.*, Phys. Rev. Lett. **102**, 027001 (2009).
 - [7] J. Yang *et al.*, Phys. Rev. Lett. **102**, 187003 (2009).
 - [8] Q. Si and E. Abrahams, Phys. Rev. Lett. **101**, 076401 (2008).
 - [9] Q. Si, E. Abrahams, J. Dai, and J.-X. Zhu, New J. Phys. **11**, 045001 (2009); Q. Si, Nat. Phys. **5**, 629 (2009).
 - [10] A. Kutepov A, K. Haule, S. Y. Savrasov, and G. Kotliar, Phys. Rev. B **82**, 045105 (2010).
 - [11] J. Guo *et al.*, Phys. Rev. B **82**, 180520 (2010).
 - [12] M. Fang *et al.*, arXiv:1012.5236.
 - [13] Z. Wang *et al.*, arXiv:1101.2059.
 - [14] Z. G. Chen *et al.*, arXiv:1101.0572.
 - [15] J.-X. Zhu *et al.*, Phys. Rev. Lett. **104**, 216405 (2010).
 - [16] C. Chao and J. Dai, arXiv:1101.0533.
 - [17] Y. Zhang *et al.*, arXiv:1012.5980.
 - [18] T. Qian *et al.*, arXiv:1012.6017.
 - [19] X-W Yan *et al.*, arXiv:1012.5536.
 - [20] C. Chao and J. Dai, arXiv:1012.5621.
 - [21] L. Zhang and D. J. Singh, Phys. Rev. B **79**, 094528 (2009).
 - [22] S. Raghu *et al.*, Phys. Rev. B **77**, 220503(R) (2008).
 - [23] S. Graser *et al.*, New J. of Phys. **11**, 025016 (2009).
 - [24] L. de'Medici, A. Georges, and S. Biermann, Phys. Rev. B **72**, 205124 (2005).
 - [25] R. Yu and Q. Si, arXiv:1006.2337.
 - [26] S. Florence and A. Georges, Phys. Rev. B **70**, 035114 (2004).
 - [27] E. Zhao and A. Paramekanti, Phys. Rev. B **76**, 195101 (2007).
 - [28] J. Orenstein *et al.*, Phys. Rev. B **42**, 6342 (1990).
 - [29] L. Haggstrom and A. Seidel, J. Magn. Magn. Mater. **98**, 37 (1991).